THE JOURNAL OF PHYSICAL CHEMISTRY C
A JOURNAL OF THE AMERICAN CHEMICAL SOCIETY

pubs.acs.org/JPCC

Article

Radiolytic Production of Radical Species in Gibbsite Doped with Iron and Chromium Ions

Hanna Hlushko, Alejandro Ramos-Ballesteros, Amita Bedar, Ping Chen, Xin Zhang, Roberto Colina Ruiz, Kevin M. Rosso, Carolyn Pearce, and Jay A. LaVerne*

Cite This: https://doi.org/10.1021/acs.jpcc.5c05004

Read Online

ACCESS | Metrics & More | Article Recommendations | Supporting Information

ABSTRACT: Gibbsite (aluminum hydroxide, $Al(OH)_3$) nanoparticles, synthesized from aluminum chloride or aluminum nitrate, were doped with metal ions, Cr(III) or Fe(III), and then irradiated with γ rays to determine the effect of the dopants on radiolytic hydrogen (H_2) production and radical generation. The addition of Cr(III) and Fe(III) ions at concentrations of 0.5% or 5% decreased the concentration of stable oxygen-centered radicals, with the strongest suppression in Cr(III) doped samples. A decrease in H_2 yields was observed with increasing Cr(III) or Fe(III) concentrations, with the greatest effect observed for the Fe(III)-doped samples. Reduction of the Cr(III) to Cr(II) and Fe(III) to Fe(II) was also observed, probably due to scavenging of radiolytically produced electrons. However, further processes differ for Fe(III)- and Cr(III)-doped systems. Both ions are reduced by the free electrons, leading to a decrease in H_2 production, but they react differently with the oxygen radicals. Cr(III) can be oxidized by oxygen radicals, whereas Fe(III) cannot. Fe(II) can interact with peroxides, possible products of intermediate oxygen oxidation, converting back to Fe(III) and leaving oxygen radicals behind. These oxidation reactions lead to a difference in the observed relative effects on H_2 yields and oxygen radical production between Cr(III)- and Fe(III)-doped gibbsite. The connection between electron scavenging and H_2 production indicates that radiolytically produced electrons are precursors to H_2.

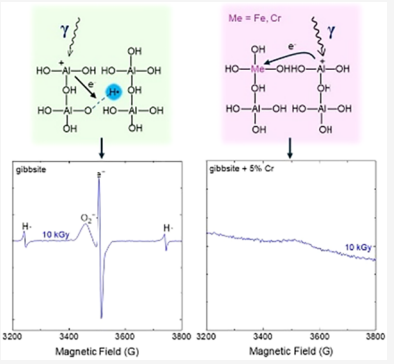

INTRODUCTION

Aluminum (oxy)hydroxide minerals, boehmite (γ-AlOOH) and gibbsite (γ-$Al(OH)_3$, sometimes named as α-$Al(OH)_3$), formed by the corrosion of aluminum from spent nuclear fuel cladding, pose a significant challenge to the treatment of highly radioactive waste stored in tanks at the Hanford, WA, site.[1] To remove waste from a tank, particles must be mobilized from their settled condition by sluicing and must remain suspended for a sufficient time to be transferred out of the tank. This process is impeded by large agglomerates of gibbsite[2] that have formed under these extreme tank waste conditions.[3] High radiation fields can generate molecular hydrogen, H_2, from water molecules associated with aluminum-bearing minerals,[4−8] which can lead to the formation of an explosive mixture with air to create an additional hazard. In addition, Hanford tank waste also has high concentrations of salts that may affect the radiolysis of gibbsite in unpredictable ways. To facilitate the safe storage and retrieval of the radioactive waste, there is a need for the assessment of gibbsite radiolysis under conditions more representative of actual tank waste.

H atom precursors to H_2 are formed from boehmite and gibbsite by the radiolytic decomposition of hydroxyl groups and adsorbed water.[9−12] H atoms and other radicals formed by radiolysis or other oxidation processes can be readily detected using electron paramagnetic resonance (EPR) spectroscopy because of their characteristic hyperfine splitting and coupling constant.[13] H atoms trapped in interstitial sites have long been observed in boehmite and more recently in gibbsite.[14−16] The most common stable radicals formed in the radiolysis of boehmite or gibbsite are oxygen species,[16−19] typically assigned to paramagnetic centers of O^- and possible O_2^- or O_3^- species.[17,18] Initial ionization in radiolysis leads to the formation of free electrons and holes. The combination mainly follows; however, the electrons that escape combination can become trapped in anionic vacancies (F-centers) and can be detected by EPR.[20] The type and stability of transients (and consequently the molecular products) induced by ionizing radiation depend on the composition, crystal structure, packing, dose rate, and temperature. They are particularly affected by the presence of impurities, such as polyvalent transition metals.[21] While radical scavenging is extensively studied in the liquid phase due to the high mobility of species, scavenging effects can also play a significant role in the solid phase. For instance, nitrate (NO_3^-) impurities present in gibbsite, arising from the aluminum nitrate used as a synthesis

Received: July 18, 2025
Revised: August 26, 2025
Accepted: August 27, 2025

precursor, can inhibit the formation of trapped hydrogen atoms,[14] hereby altering radiolytic pathways and yields. It is important to note that the presence of nitrates is expected in the chemical environment of the waste tanks at Hanford.[22] Therefore, solid-state radiolysis studies in the presence of nitrates are essential to understanding and modeling the speciation and chemical changes in storage tanks. In this investigation, we conducted solid-state radiolysis and characterization studies on gibbsite derived from chloride and nitrate precursors.

Iron (Fe) and chromium (Cr) are the most abundant transition metals in the Hanford site waste,[23] and recent work has shown that trace amounts of these ions can be incorporated into the gibbsite crystal structure during coprecipitation[24] or adsorbed onto gibbsite surfaces through interactions with six different gibbsite hydroxyls.[25] Previous studies have confirmed that the presence of small quantities of Cr(III) can hinder both gibbsite and boehmite dissolution.[24,26] This inhibition mechanism involves the adsorption of Cr clusters onto gibbsite and boehmite, leading to the partial passivation of the surface.[27,28]

The research reported here focuses on the γ radiolysis of gibbsite synthesized from aluminum chloride and aluminum nitrate precursors and doped with different concentrations of Cr(III) or Fe(III) to better understand the role of impurities in the radiolytic behavior of gibbsite. EPR was used to measure the stable radical species. Diffuse-reflectance spectroscopy techniques were used to reveal local structure changes, while X-ray diffraction was used to observe long-range effects. H_2 produced during gibbsite radiolysis was analyzed using gas chromatography techniques.

MATERIALS AND METHODS

Material synthesis was performed using a hydrothermal technique, as published previously.[23,29] Briefly, 0.25 M solutions of $AlCl_3$ or $Al(NO_3)_3$ were made using deionized (DI) water, and the pH was adjusted to about 5 with a 3 M NaOH solution under constant mixing. Once amorphous aluminum hydroxide was formed, the suspension was stirred continuously for 1 h. The resulting precipitate was then collected by centrifugation. The precipitate was washed three times with DI water and subsequently redispersed in DI water for hydrothermal treatment. For the synthesis of trace metal-doped gibbsite, appropriate amounts of $CrCl_3$ or $FeCl_3$ in the $AlCl_3$ solutions and $Cr(NO_3)_3$ or $Fe(NO_3)_3$ in the $Al(NO_3)_3$ solutions were added in quantities calculated to yield mixed hydroxides containing 0.5% and 5% Fe(III) or Cr(III), respectively. No further characterizations of the final doped gibbsites were made, and it is assumed that the final concentrations of dopants are as predicted. After the addition of extra metal ions, the mixture was stirred at 80 °C for 7 days. Formed gibbsite platelets were washed three times in DI water with consequent centrifugation at 10,000 rpm and dried at 80 °C overnight in an electrical oven.

Irradiations were performed at the Radiation Laboratory of the University of Notre Dame using a contained ^{60}Co source with a dose rate of ~50 Gy/min. Samples were flame-sealed in quartz Suprasil tubes under vacuum, and irradiated to 1, 5, 10, and 20 kGy, for EPR and diffuse-reflectance measurements. The samples for H_2 measurements were flame-sealed in Pyrex tubes (10 mm diameter by about 10 cm long) under vacuum and irradiated to 500 kGy. The dose was determined based on Fricke dosimetry and adjusted for natural ^{60}Co decay.

Diffuse-reflectance infrared Fourier transform spectroscopy (DRIFTS) was performed with a Bruker Vertex 70 spectrometer equipped with a DGTS detector and Harrick Praying Mantis high-temperature cell. Spectra were collected from 400 to 4000 cm^{-1} wavenumbers with steps of 4 cm^{-1}. The spectrum of KBr collected at 400 °C was used for the background.

Diffuse-reflectance UV−visible optical spectroscopy was performed with a Flame−S-UV−vis Ocean Optics spectrometer equipped with an Ocean Optics reflection probe R400−7-Vis/NIR at 45° (six illumination fibers and one detector) coupled with an Ocean Optics DH-2000-BAL deuterium-tungsten light source. Duplicate spectra were collected from three distinct regions of the sample to enhance the representativeness. Each spectrum was an average of 10 scans with an integration time of 1700 ms. Optical grade poly(tetrafluoroethylene) (PTFE), packed in a tube identical to those used for the samples, was employed as a reference. Relative absorbance spectra were obtained from reflectance spectra treated with a Kubelka−Munk model.

Gibbsite particles were imaged by using scanning electron microscopy (SEM) with a Magellan 400 field emission scanning electron microscope. The beam current used for imaging was 25 pA, and the beam voltage was 5 kV. The powders of interest were spread over conductive carbon tape and sputtered with 3 nm of Pt/Pd coating prior to the imaging.

Gibbsite surface chemistry was characterized by X-ray photoelectron spectroscopy (XPS) using a PHI VersaProbe II instrument equipped with an Al−Kα X-ray source with a photon energy of 1486.6 eV. Individual element high-resolution scans were collected at a pass energy of 23 eV and energy steps of 0.1 eV. Flooding the chamber with 10 eV Ar^{2+} ions and low-energy electrons was used to minimize surface charging. All energy values of the spectra were shifted to match the C 1s peak at 284.8 eV.

Powder X-ray diffraction (pXRD) was used to confirm the crystalline structure of all synthesized materials using a high-resolution Bruker D8 Discover XRD instrument. Scans were taken in the 2θ range of 10−60° with an increment of 0.023°.

EPR spectra were obtained using a Bruker EMX spectrometer at an X-band frequency (~9.8 GHz), 30 dB attenuation, 1 G modulation amplitude, and 2 mW power. OriginLab software was used to integrate and deconvolute the peaks in the collected spectra. The characteristic resonance peaks of radiation-induced radical species in the Suprasil cells (g = 2.0001) were subtracted from the presented spectra.

Surface-sensitive Fe and Cr L-edge X-ray absorption spectroscopy (XAS) was used to assess radiation-induced changes in the oxidation state of the ions. Data were collected on a Beamline 4.0.2 at the Advanced Light Source (Lawrence Berkeley National Laboratory, CA). Sealed quartz tubes containing the irradiated gibbsite were opened in a nitrogen-filled glovebox. The synthesized and irradiated powdered samples were pressed into an indium foil and mounted onto a copper probe by using silver paint. The sample holder was then sealed into an anaerobic container for shipment and removed immediately prior to insertion into the nitrogen-filled end-station. X-ray absorption (XA) spectra at the Fe and Cr $L_{2,3}$ edges were collected in total electron yield (TEY) mode with an effective probing depth of 50 Å.[30]

The yield of H_2 gas produced in each sample was measured using an SRI 8610 gas chromatograph with a thermal conductivity detector and an argon carrier gas. Following

https://doi.org/10.1021/acs.jpcc.5c05004
J. Phys. Chem. C XXXX, XXX, XXX−XXX

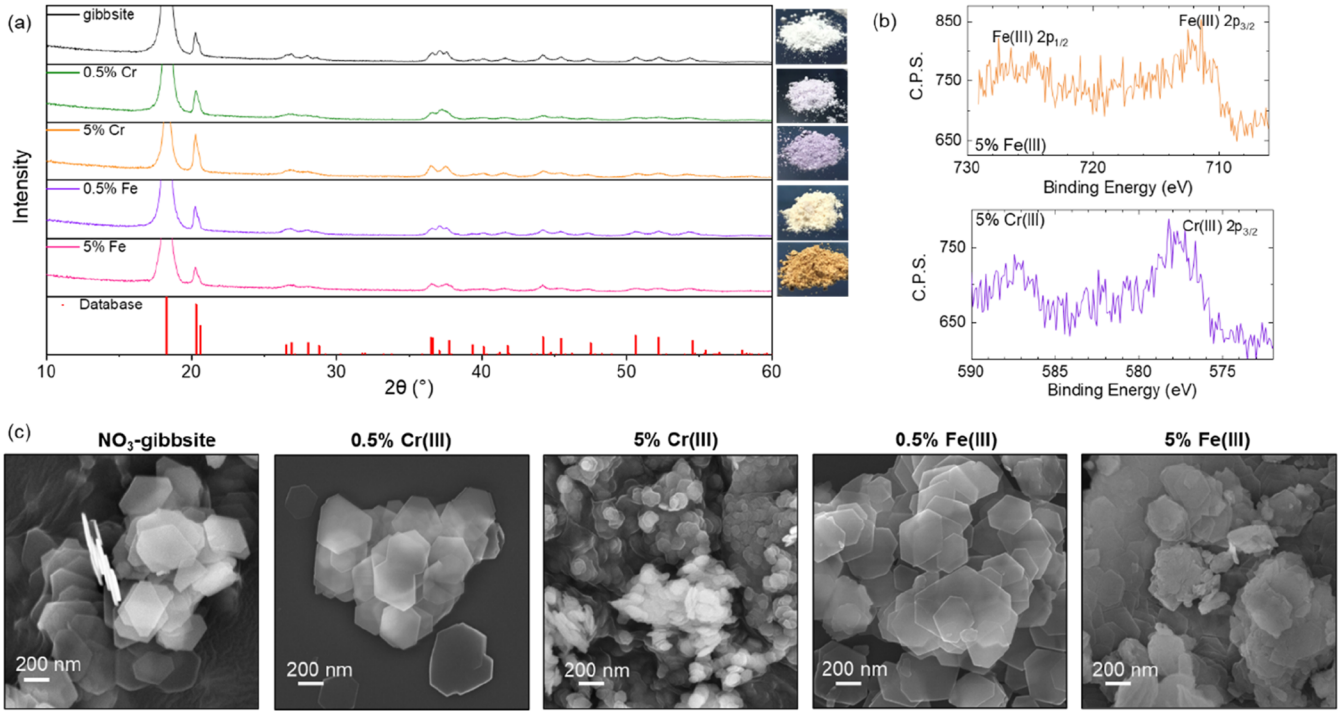

Figure 1. (a) pXRD patterns of undoped NO_3-gibbsite and NO_3-gibbsite doped with Fe(III) or Cr(III) with photographs of the powders on the right, (b) high-resolution XPS spectra of Fe(III) in 5% Fe(III)-doped gibbsite (top) and Cr(III) in 5% Cr(III)-doped NO_3-gibbsite (bottom), and (c) SEM micrographs of undoped and doped NO_3-gibbsite platelets.

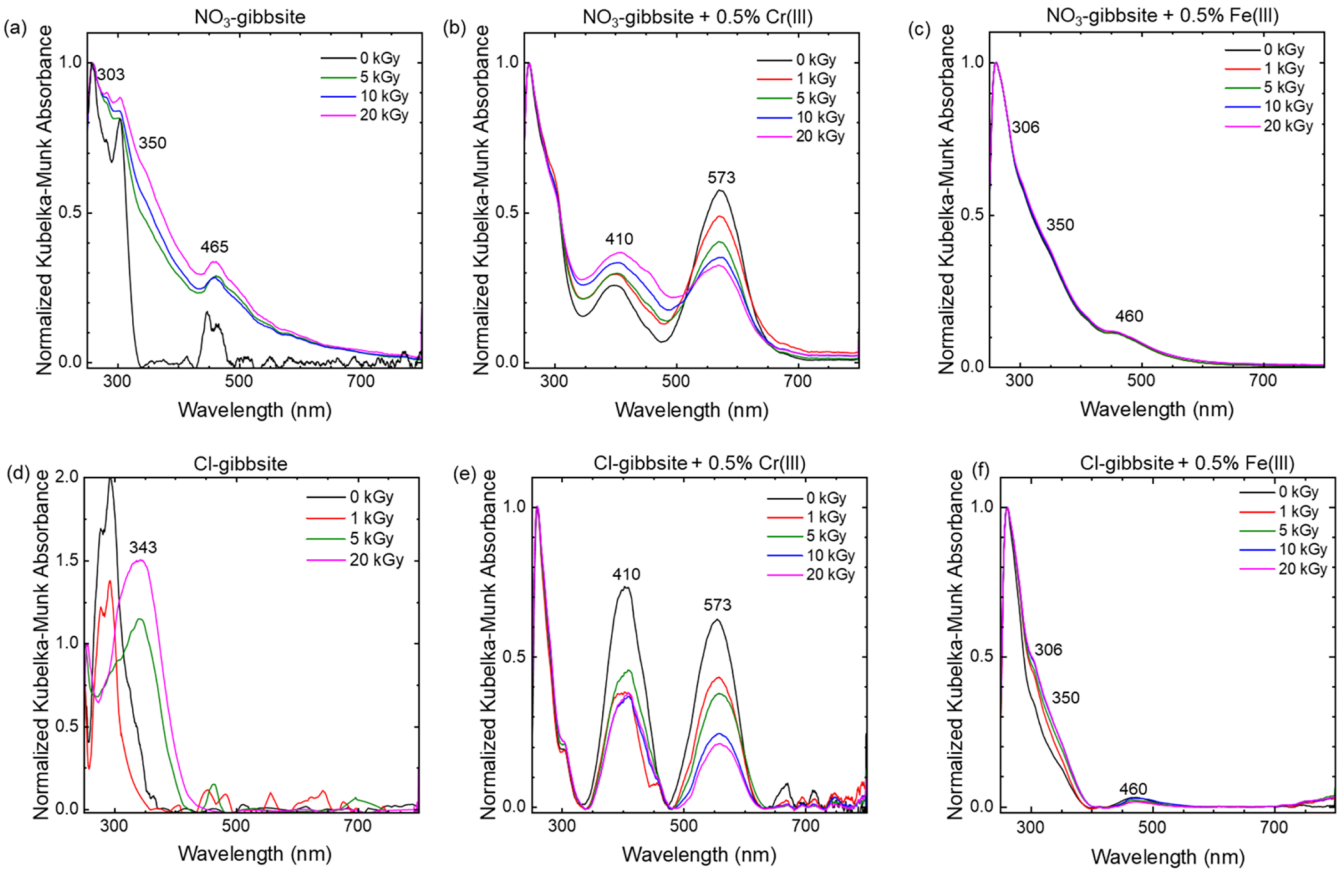

Figure 2. Diffuse-reflectance UV−visible spectra treated with Kubelka−Munk transformation of as-synthesized and irradiated NO_3-gibbsite (a), NO_3-gibbsite with 0.5% Cr(III) (b) and 0.5% Fe (c), Cl-gibbsite (d), and Cl-gibbsite with 0.5% Cr(III) (e) and 0.5% Fe(III) (f).

https://doi.org/10.1021/acs.jpcc.5c05004
J. Phys. Chem. C XXXX, XXX, XXX−XXX

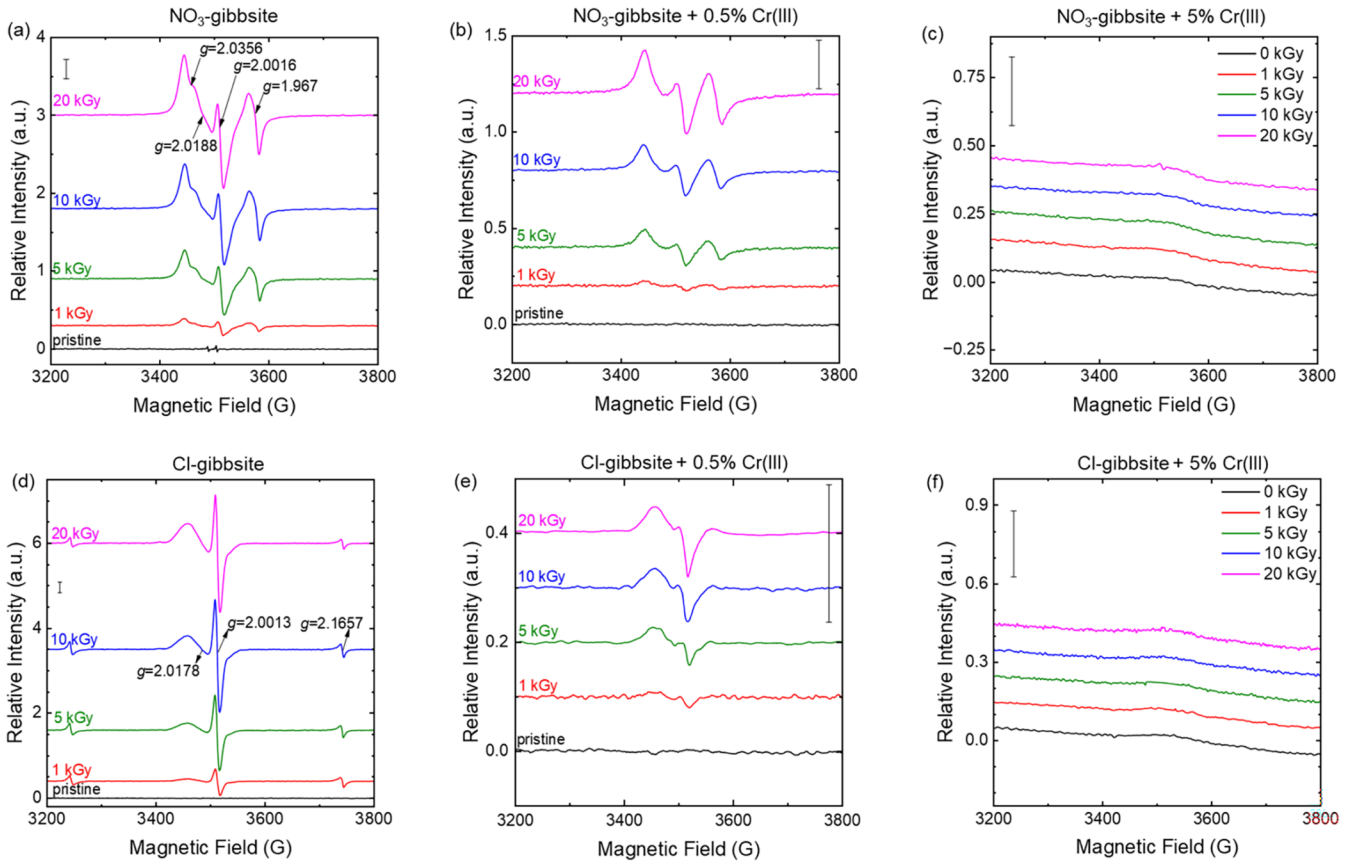

Figure 3. EPR spectra of (a) irradiated undoped NO_3-gibbsite, (b) NO_3-gibbsite doped with 0.5% Cr(III), (c) NO_3-gibbsite doped with 5% Cr(III), (d) undoped Cl-gibbsite, (e) Cl-gibbsite doped with 0.5% Cr(III), and (f) Cl-gibbsite doped with 5% Cr(III).

irradiation, the samples were inserted into a flexible PVC tube that was connected to the chromatograph by a four-way valve, flushed with the carrier gas, and cracked open to allow for the measurement of H_2. Calibration of H_2 was performed by injecting a fixed amount of gas using a gastight syringe.

RESULTS

Characterization of As-Synthesized Undoped and Doped Gibbsite. Gibbsite was hydrothermally synthesized from (i) aluminum chloride (Cl-gibbsite) and (ii) aluminum nitrate (NO_3-gibbsite). Previous Fe and Cr K-edge extended X-ray absorption fine structure spectroscopy showed that Fe(III) or Cr(III) ions were incorporated into the crystalline gibbsite structure when synthesized following this procedure.[24,31] High-resolution oxygen 1s and aluminum 2p XPS data for undoped NO_3-gibbsite and for Fe(III)- and Cr(III)-doped NO_3-gibbsite (Figure S1) show that doping did not significantly change the oxygen and aluminum speciation at the surface. The similarity of the pXRD patterns for the undoped and doped materials (Figure 1a) suggests that no new crystalline phases were formed upon doping, and incorporation of Fe(III) and Cr(III), which have similar size and charge to Al(III), did not significantly change the crystal structure of gibbsite. However, at a doping level of 5% Fe(III) or Cr(III), the peak at 18.3° 2θ corresponding to the (002) plane broadens (Figure S2), suggesting either a decrease in the size of the platelets or more disorder in the interlayer spacing. SEM images (Figure 1b) reveal that the platelet morphology and size (300−400 nm in diameter) of gibbsite doped with 0.5% of Fe(III) or Cr(III) are the same as those for undoped gibbsite, which agrees well with our previous study.[23] Increasing the doping level to 5% resulted in some changes, with Fe(III)-doped gibbsite platelets having more edge defects and Cr(III)-doped gibbsite platelets decreasing in size, as suggested by SEM (Figure 1C). At a doping level of 5%, XPS analysis confirmed that the iron and chromium ions present on the gibbsite surface remained in the +3 oxidation state (Figure 1b), consistent with the oxidation states typically observed in Cr(III)- or Fe(III)-adsorbed gibbsite minerals. While undoped gibbsite is white, doped materials developed color characteristics to Fe(III) and Cr(III), yellow and purple, respectively, which intensified as the dopant concentration increased (Figure 1a).

DRIFTS did not reveal significant differences between undoped and doped NO_3-gibbsite (Figure S1c), suggesting that Fe(III) or Cr(III) ions substitute for Al(III) in the matrix and are connected through hydroxyl groups or oxygen bridges. The DRIFTS spectra for undoped and doped NO_3-gibbsite showed a band at 1380 nm, which can be attributed to the residual nitrate ions from the synthesis. The presence of nitrate ions was also confirmed with diffuse-reflectance optical spectroscopy (Figure 2a), EPR (Figure S4), and XPS (Figure S5). The XPS peak for nitrogen at 408 eV corresponding to NO_3^- is fully removed from the surface after sputtering with He ions. This suggests that sputtering causes partial reduction of NO_3^- into gaseous products that desorb quickly, which has previously been observed in XPS studies.[32] No NO_3^- peaks were observed in undoped Cl-gibbsite, which was characterized previously,[14] but it did contain some residual chloride.

https://doi.org/10.1021/acs.jpcc.5c05004
J. Phys. Chem. C XXXX, XXX, XXX−XXX

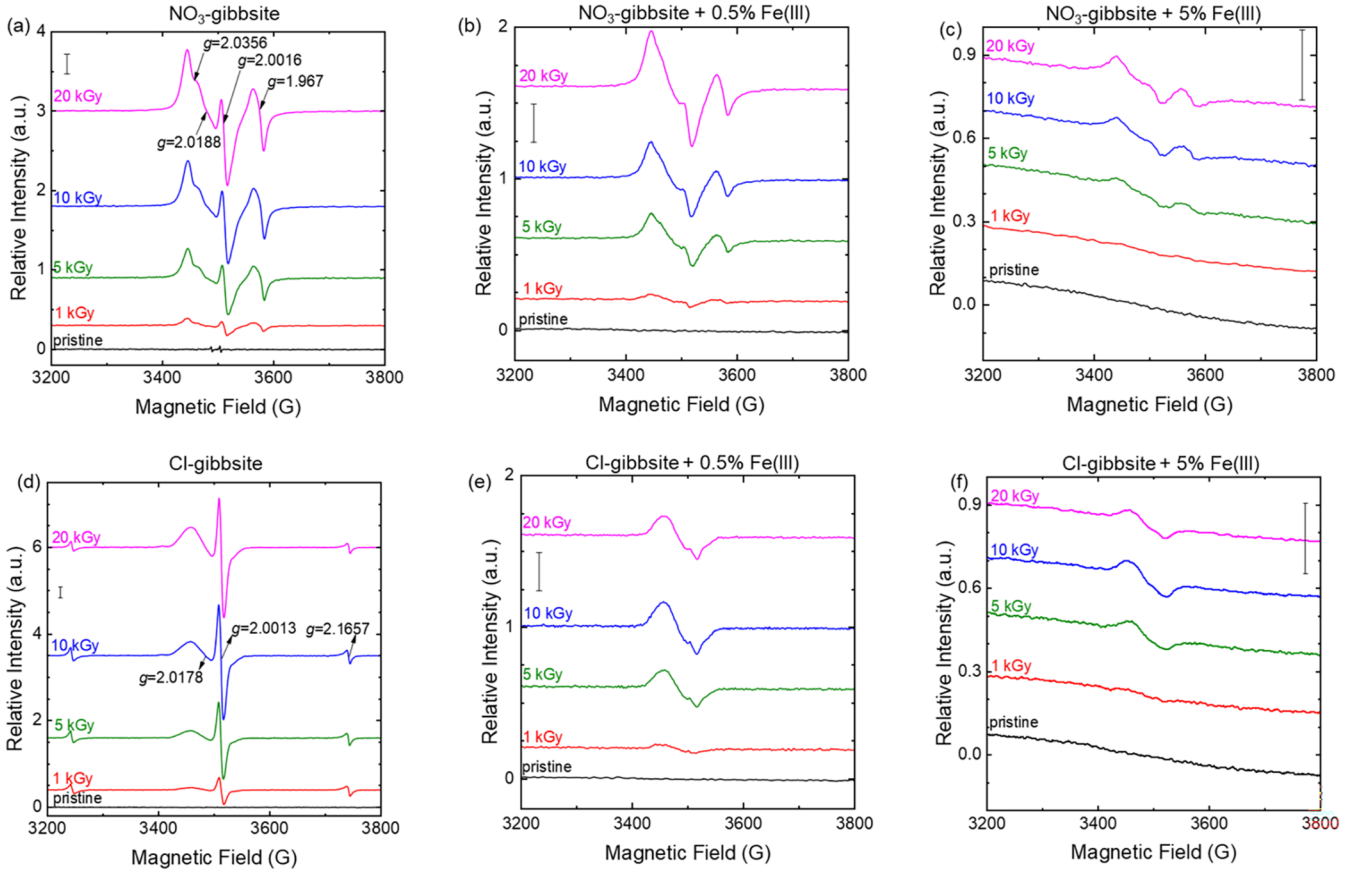

Figure 4. EPR spectra of (a) irradiated undoped NO_3-gibbsite, (b) NO_3-gibbsite doped with 0.5% Fe(III), (c) NO_3-gibbsite doped with 5% Fe(III), (d) undoped Cl-gibbsite, (e) Cl-gibbsite doped with 0.5% Fe(III), and (f) Cl-gibbsite doped with 5% Fe(III).

Characterization of Irradiated Undoped and Doped Gibbsite. The effect of the dopants on the formation of radiolytic products under ^{60}Co γ irradiation was studied with UV−visible diffuse reflectance and EPR. All absorption spectra consistently show the tail of the fundamental band around 260 nm. This peak was chosen to normalize all of the spectra, allowing for the subtraction of the background effect that rises with irradiation and thereby revealing radiation-induced chemical changes. Before irradiation, the UV−visible region of the diffuse-reflectance spectrum for undoped NO_3-gibbsite (Figure 2a, black spectrum) had a peak at 303 nm, which was previously attributed to the absorption bands of NO_3^- in aluminum nitrate solutions[33] and saturated sodium nitrate solutions and melts,[34] so it can belong to residual nitroxide species in NO_3-gibbsite. This assignment is supported by the sharp triplet in the EPR spectrum for NO_3-gibbsite before irradiation (Figure S4), which is assigned to the nitrogen dioxide radical ($^{\bullet}NO_2$) that can form in small amounts from nitrate decomposition. Before irradiation, the diffuse-reflectance spectrum for undoped Cl-gibbsite (Figure 2d, black spectrum) had peaks at 295 nm, which could be due to the residual chloride species ($Cl^{\bullet}$ or Cl_3^-), and it decreased upon irradiation. A similar peak was reported in γ-irradiated KCl (Cl_3^- at 232 and 235 nm).[35] The EPR spectrum of unirradiated Cl-gibbsite (Figure S4) also contains a very small yet pronounced signal with g = 2.0032 and g = 2.019, and a splitting of 2.42 mT, which is likely due to chloride radicals or oxychloride radicals ($ClOO^{\bullet}$). After irradiation, the peak at 350 nm in the UV−visible diffuse-reflectance spectra for NO_3-gibbsite increases in intensity with an increasing dose. There is a very small increase in the shoulder at 350 nm in doped samples as well. Irradiation of Cl-gibbsite results in a broad peak at ∼343 nm, while a small shoulder increases with increasing dose in the spectra of Cl-gibbsite doped with Fe(III). Since all studied materials develop a peak of various intensities around 350 nm when irradiated, it is reasonable to suggest that this peak corresponds to the superoxide radical, as it is the only common radical species observed in all irradiated gibbsites (Figure 2). This species presumably occurs by breaking two nearby O−H bonds followed by the coupling of the residual bound O- species, as previously proposed.[17,20] Gibbsite was not fully dried, and some surface water might still be present, which could also be a source of the superoxide radical. A superoxide peak in solid KO_2 was observed at 350 nm,[36] which supports the proposed assignment. A similar peak was observed in kinetic studies of chlorite−chloride reactions.[37] ClO_2 was reported at 358 nm, while Cl_2 and Cl^- were reported to have weaker peaks at ∼325 nm. However, the EPR spectrum of irradiated Cl-gibbsite (Figure 3d) did not have peaks that could be assigned to chlorine-centered radicals, since they did not demonstrate typical splitting attributed to the isotopic composition of chlorine, so the observed 343 nm peak is more likely due to the superoxide radical or molecular oxychloride species that are not radicals.

Diffuse-reflectance UV−visible spectra for Cr-doped NO_3-gibbsite (Figure 2c, Figure S3) had peaks at 410 and 573−574 nm, which correspond to d−d electron transitions of Cr(III) ions.[38,39] Previous studies of Cr(III) hydrolysis established a

https://doi.org/10.1021/acs.jpcc.5c05004
J. Phys. Chem. C XXXX, XXX, XXX−XXX

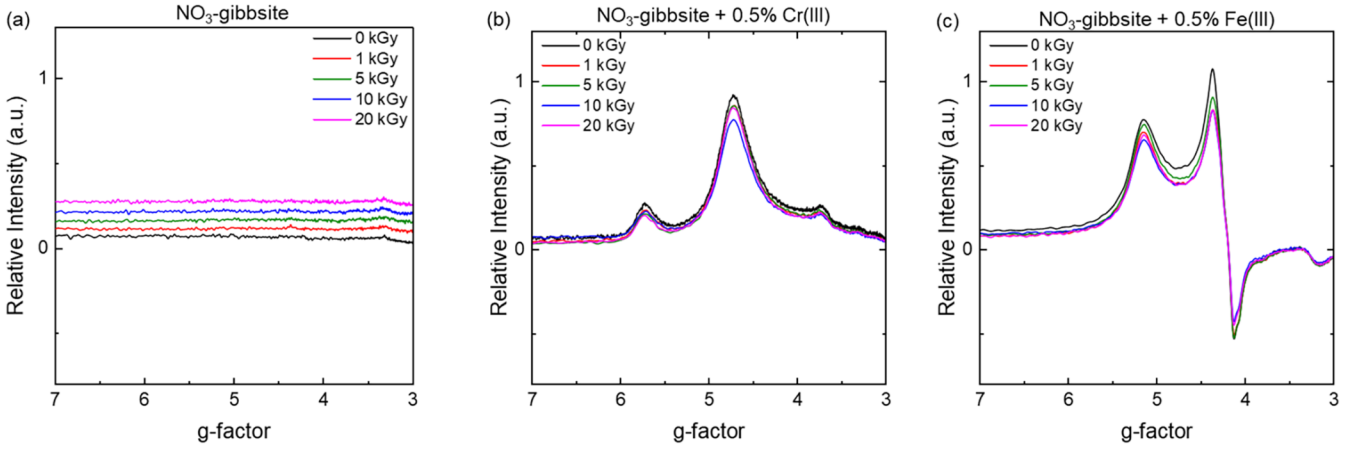

Figure 5. Low-field EPR spectra of (a) NO_3-gibbsite, (b) NO_3-gibbsite with 0.5% Cr(III), and (c) NO_3-gibbsite with 0.5% Fe(III).

bathochromic shift of the peaks, from 408 and 575 nm for monomeric Cr^{3+} in the solution, to 426 and 580 nm for tetramers ($Cr_4(OH)_6^{6+}$).[40] The peak positions in Figure 2c suggest that Cr(III) ions are more likely dispersed within the gibbsite structure and do not cluster, even at the higher dopant level (Figure S3). The difference in relative intensity between the peak for gibbsite at 260 nm and the peak for Cr(III) ions at 575 nm shows that there is a higher Cr(III) concentration in the NO_3-gibbsite sample doped with 5% Cr than in the sample doped with 0.5% Cr, as expected (Figures 2b and S3a). After irradiation with the highest dose (20 kGy), there is a decrease in intensity of the peak at 573−574 nm, suggesting that radiation decreases the concentration of Cr(III) ions. Besides, the peak at 410 nm shows broadening with the dose, which is indicative of a wider distribution of transitions due to changes in the ligand field symmetry (interaction). The latter can be changes in coordination or bond length. Diffuse-reflectance UV−visible spectra for 0.5% Fe-doped NO_3-gibbsite Fe(III) ions had a broad peak with several shoulders in the region between 250 and 350 nm, corresponding to the absorbance of Fe(III) ions. Except for the shoulder at 350 nm, after the spectra were normalized, no major changes on irradiation were noticeable.

The EPR spectra of Cl-gibbsite and NO_3-gibbsite are shown with Cr(III) doping in Figure 3 and Fe(III) doping in Figure 4. Radiolysis led to the production of at least five discernible peaks, three of which were assigned to the $^{\bullet}NO_2$ radical (g_1 = 1.9676, $FWHM_1$ = 0.0143, g_2 = 2.0016, $FWHM_2$ = 0.0129, and g_3 = 2.0356, $fwhm_3$ = 0.0136 and A = 6 mT)[14] (Figure 3a), which can be formed from radiolytic decomposition of NO_3^-.[41] The peak with g = 2.0188 and FWHM = 0.0308 was assigned to $O_2^{\bullet-}$. Formation of $O_2^{\bullet-}$ was detected at a similar position in EPR during high-temperature decomposition of $NaNO_2$ and $NaNO_3$ and characterized by the g factor between 2.0169 and 2.0115 depending on the radical environment.[34] A peak at a similar position was observed in magnesium oxide[42] and titanium oxide,[43] treated with hydrogen peroxide. The small peak with a g factor of 2.001, FWHM = 0.00702, was assigned to residual F-centers. The intensity of these peaks increased with dose, reaching saturation after 10 kGy. The peaks corresponding to $^{\bullet}NO_2$ radicals were present in the spectra for all irradiated NO_3-gibbsite samples, even after a sealed sample was heated up to 200 °C post radiolysis (data not shown). The peaks for the same radical species were present in the EPR spectra for both doped and undoped NO_3-gibbsite, but with different intensities that were affected by the nature and concentration of the dopant. With increasing concentration of Cr(III) ions, there is a decrease in the intensity of the peaks corresponding to oxygen-containing species, as well as an overall decrease of radical spin density in samples receiving the same dose.

Similar effects on the amount of radical formation with variations in dopant concentration were observed in Cl-gibbsite and NO_3-gibbsite (Figures 3 and 4). In gibbsite doped with 5% Cr(III) or 5% Fe(III), almost no radicals were detected. Gibbsite doped with Fe(III) showed more trapped radicals than gibbsite doped with Cr(III). For NO_3-gibbsite, doping with either Cr(III) or Fe(III) suppressed the peak corresponding to the $O_2^{\bullet-}$ radicals to a greater extent than the peak corresponding to $^{\bullet}NO_2$. For Cl-gibbsite, doping with either Cr(III) or Fe(III) suppressed the peak corresponding to F-centers (g = 2.0013, FWHM = 0.00702) over the peak corresponding to $O_2^{\bullet-}$ (g = 2.0188, FWHM = 0.0308). Doping either NO_3-gibbsite or Cl-gibbsite with Cr(III) or Fe(III) fully suppressed trapped $H^{\bullet}$ atoms, and Cl-gibbsite was the only material that had detectable trapped $H^{\bullet}$ atoms (g = 2.1657, FWHM = 0.00695 and g = 1.8785, FWHM = 0.00572).

Fe(III) and Cr(III) are transition-metal ions with several unpaired electrons in 3d-orbitals that are responsible for the zero-field splitting in the low-field EPR spectra (Figure 5). Undoped NO_3-gibbsite did not have any peaks in this area, suggesting the absence of 3D-metal ion impurities (Figure 5a). The shape of the Fe(III) and Cr(III) low-field spectra suggests that the dopants in gibbsite adopt an orthorhombic configuration with $g_x \neq g_y \neq g_z$.[44,45] The positions and shapes of the peaks do not change after irradiation, suggesting that the local environments of the Fe(III) and Cr(III) ions are not changed by radiolysis. However, there are some changes in the intensity of the peaks after irradiation, suggesting some changes in the concentration of transition-metal ions in the gibbsite.

Fe and Cr $L_{2,3}$-edge (2p − 3d transition) XAS data were collected to determine if there were any radiation-induced changes to the oxidation state of the Cr(III) or Fe(III) ions. NO_3-gibbsite samples doped with either 5% Cr(III) or 5% Fe(III) were irradiated to a higher dose of 500 kGy to maximize any radiation-induced effects. Samples were manipulated in an inert atmosphere to remove any potential for reoxidation after irradiation. The Cr $L_{2,3}$-edge XA spectra for the NO_3-gibbsite doped with 5% Cr before and after

https://doi.org/10.1021/acs.jpcc.5c05004
J. Phys. Chem. C XXXX, XXX, XXX−XXX

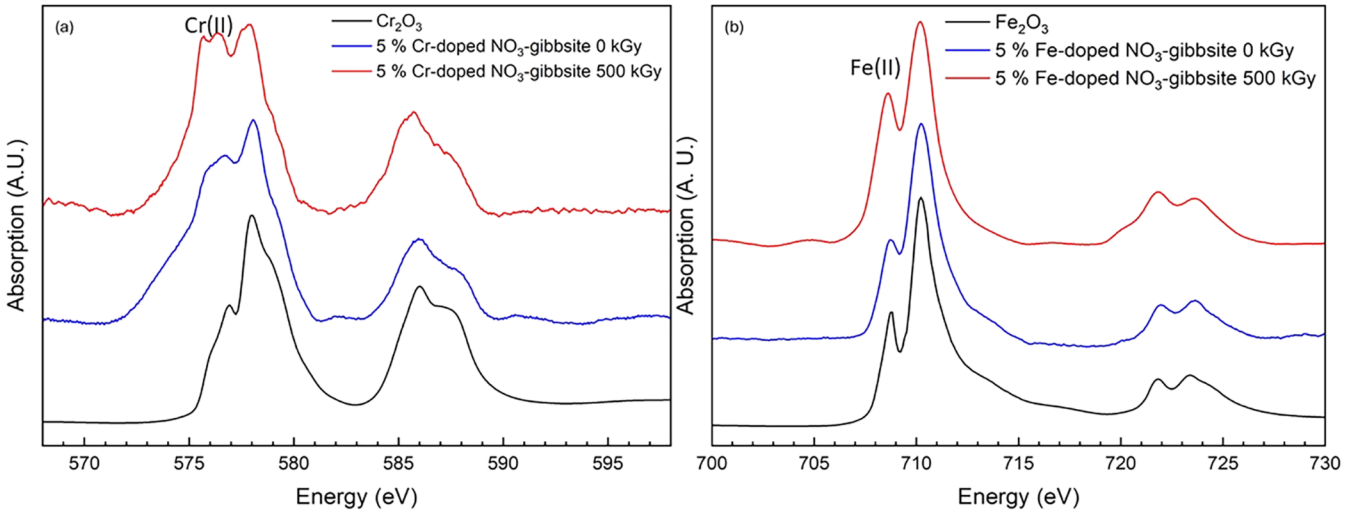

Figure 6. (a) Cr $L_{2,3}$-edge XA spectra of NO_3-gibbsite doped with 5% Cr before (blue) and after (red) ^{60}Co γ irradiation (500 kGy) and of eskolaite (Cr_2O_3) as a Cr(III) standard (black). (b) Fe $L_{2,3}$-edge XA spectra of NO_3-gibbsite doped with 5% Fe before (blue) and after (red) ^{60}Co γ irradiation (500 kGy) and of hematite (Fe_2O_3) as a Fe(III) standard (black).

irradiation have a peak at the same energy position as that of the Cr(III) standard eskolaite (Cr_2O_3), confirming the Cr(III) oxidation state (Figure 6a). However, there is an increase in intensity of the peaks at lower energy in the XA spectrum for the sample after irradiation (500 kGy), suggesting some reduction of Cr(III) to Cr(II).[46] The Fe $L_{2,3}$-edge XA spectra for the NO_3-gibbsite doped with 5% Fe before and after irradiation have a peak at the same energy position as that of the Fe(III) standard hematite (Fe_2O_3), confirming the Fe(III) oxidation state (Figure 6b). As with the Cr(III)-doped gibbsite, the XA spectrum for the Fe(III)-doped gibbsite after irradiation (500 kGy), shows an increase in intensity of the lower energy peak, suggesting that irradiation also induced some reduction of Fe(III) to Fe(II).[47]

H_2 gas evolved as a radiolytic species from the irradiation of boehmite and gibbsite.[17,18,48,49] The production of H_2 from NO_3-gibbsite, Cl-gibbsite, and Cl-gibbsite doped with different concentrations of Cr(III) or Fe(III) is shown in Figure 7. The yield of H_2 from the radiolysis of Cl-gibbsite is about an order of magnitude greater than the yield of H_2 from the radiolysis of NO_3-gibbsite. Doping the Cl-gibbsite with either Cr(III) or Fe(III) inhibited the formation of H_2, with Fe(III) having a greater effect than Cr(III). Increasing the amount of Cr(III) or Fe(III) in the doped Cl-gibbsite resulted in a reduction of H_2 yields.

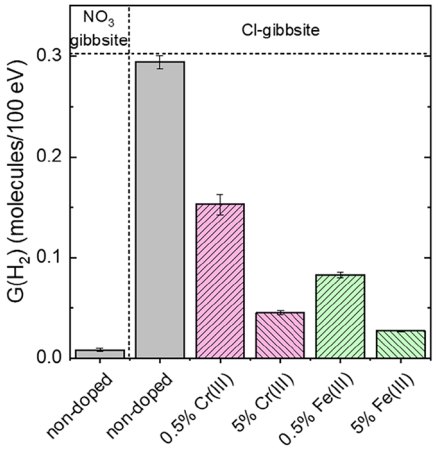

Figure 7. $G(H_2)$ value for undoped NO_3-gibbsite, undoped Cl-gibbsite, and Cl-gibbsite doped with different amounts of Cr(III) and Fe(III), irradiated with 500 kGy of ^{60}Co γ radiation.

DISCUSSION

Residual precursors from the synthesis of gibbsite can be found in the final materials, including nitrate ions for NO_3-gibbsite and chlorides for Cl-gibbsite.[14] In the irradiation of undoped NO_3-gibbsite, $H^\bullet$ atoms are not observed in EPR, suggesting that they or their precursors are scavenged by the nitrate ions. Consequently, H_2 generation was much lower in the radiolysis of NO_3-gibbsite compared with Cl-gibbsite. Residual chloride ions had very little effect on the extent of H_2 production, resulting in a yield of H_2 ($G(H_2)$) for Cl-gibbsite of 0.29 molecules/100 eV deposited in the solid, which is the highest yield reported for gibbsite.[14]

EPR spectra show that radiolysis of Cl-gibbsite did not produce a significant amount of stable chloride-centered radicals, suggesting that if the chloride is oxidized by radiolysis, the products formed are not paramagnetic. A significant decrease in the radical spin density was observed in the EPR of both gibbsites doped with Cr(III) or Fe(III). Integration and deconvolution of the EPR signal of NO_3-gibbsites (Figures 8 and S6) show the difference between undoped NO_3-gibbsite and NO_3-gibbsite containing 0.5% Fe(III) or Cr(III) immediately after irradiation and 100 days after irradiation (Figure 8). Since nitrate ions form ionic bonds with Al (and/or Fe or Cr), it was assumed that the ratio between the peaks belonging to the same radical should be similar in all samples. Deconvolution revealed that the peak assigned to the O_2^- radical (g = 2.02180) has a higher intensity in the undoped sample and is significantly reduced in the doped samples, while the signal from $^\bullet NO_2$ is suppressed less. In a re-examination 100 days after irradiation, the O_2^- radical is fully decayed in the 0.5% Cr(III) sample, while the $^\bullet NO_2$ radical is highly persistent.

Figures 3 and 4 show that the addition of Cr(III) and Fe(III) fully suppressed any detectable signal from the $H^\bullet$ atom, suggesting very efficient scavenging of $H^\bullet$ atoms or their

https://doi.org/10.1021/acs.jpcc.5c05004
J. Phys. Chem. C XXXX, XXX, XXX−XXX

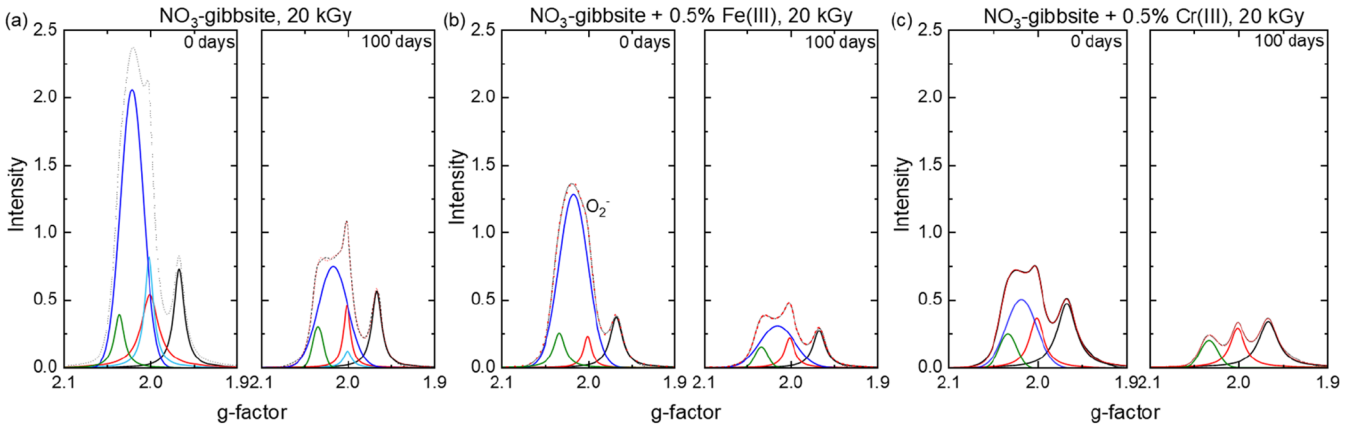

Figure 8. Deconvolution of the EPR signal collected for (a) NO_3-gibbsite, (b) NO_3-gibbsite with 0.5% Fe(III), and (c) NO_3-gibbsite with 0.5% Cr(III) irradiated with 20 kGy of ^{60}Co γ radiation immediately after irradiation (on the left) and 100 days after irradiation (on the right).

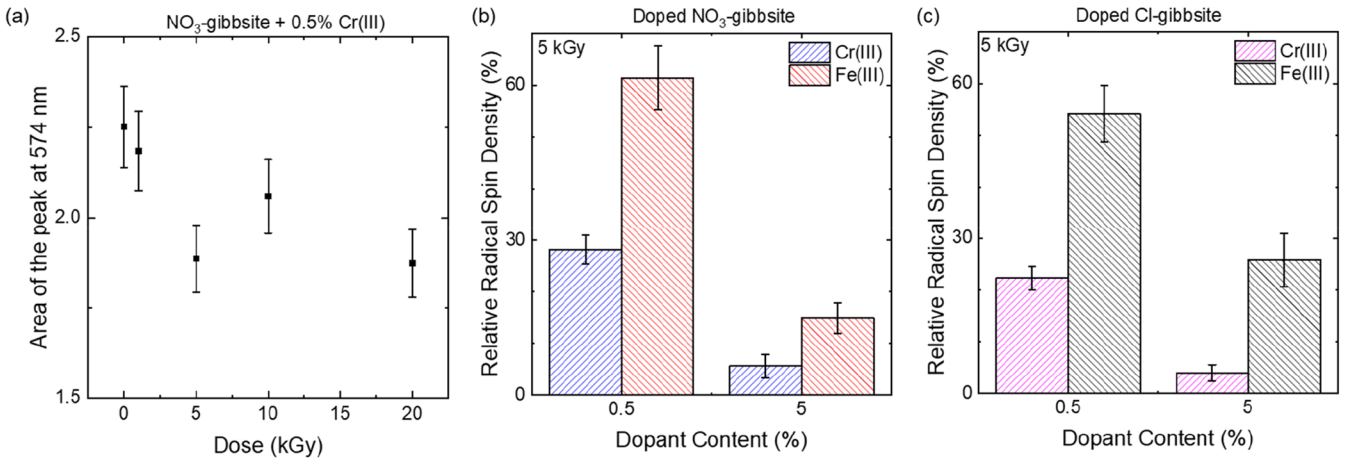

Figure 9. (a) Decrease in the area of the absorbance peak assigned to Cr(III) in diffuse-reflectance UV−visible spectra for NO_3-gibbsite with dose. Relative radical spin density of the oxygen superoxide peak induced in materials in (b) NO_3-gibbsites and (c) and of all radicals in Cl-gibbsites as a function of dopant concentration.

precursors by these 3d-metal ions. There was also a dramatic decrease in H_2 yields with doping (Figure 5). Significant scavenging of the F-center peak by the metal ion dopant suggests that they are scavenging free electrons, which are precursors of $H^{\bullet}$ atom radicals. At the same time, some evidence was found to show that metal ion reduction is likely taking place. Figure 9a shows that the area of the peak at 574 nm in the diffuse-reflectance UV−visible spectra of Cr(III)-doped gibbsites decreases with increasing irradiation dose, suggesting the reduction of Cr(III) to Cr(II). Cr and Fe $L_{2,3}$-edge XA spectra also show evidence for some reduction of Cr(III) and Fe(IIII) to Cr(II) and Fe(II) in irradiated samples. Very efficient scavenging of electrons by NO_3^- and the reduction of metal ions suggest that they both are trapping electrons. The same electron precursor must be responsible for H_2 production, as supported by its decreased yield with increasing metal dopant content.

Double integration of the EPR spectra gives the relative intensities of the O_2^- peaks for NO_3-gibbsites and the relative intensity of all radical peaks in Cl-gibbsites as a function of the amount of doped Cr(III) or Fe(III) for the samples irradiated to 5 kGy (Figure 9b,c). The intensity of peaks corresponding to O_2^- decreased with increasing metal ion dopant content. Doping NO_3-gibbsite with Cr(III) ions had a greater effect on O_2^- generation than doping with Fe(III) ions at the same concentration. The same trend is observed for Cl-gibbsite, with the total concentration of radicals decreasing more when Cr(III) is the dopant than when Fe(III) is the dopant. The difference in response may be related to the differences in electronegativity of Cr and Fe or due to better stabilization of Cr(II) in the gibbsite matrix than that of Fe(II).

The consumption of Cr(III) and Fe(III), and the fact that the $H^{\bullet}$ atom yield decrease is correlated with increasing metal ion dopant concentration, strongly implies that electrons are precursors to $H^{\bullet}$ atoms and ultimately H_2. Deposition of energy from ionizing radiation will produce free electrons and holes. Even at the highest dopant concentration, the gibbsite is mainly made up of Al, O, and H atoms that are the likely source of ionization. The role of the Cr(III) and Fe(III) must be in the scavenging of those electrons, as indicated by the observation of Cr(II) and Fe(II) following radiolysis, as shown in Figure 6. The reduction potentials for these two metals are[50]

$$Cr^{3+} + e^- \rightarrow Cr^{2+} - 0.41V$$

$$Fe^{3+} + e^- \rightarrow Fe^{2+} + 0.77V$$

so one would expect the Fe(III) to be more efficient than the Cr(III), which correlates with higher efficacy of H_2 scavenging in Fe(III)-doped samples. However, the total concentration of the radicals was always lower in Cr(III)-doped samples,

https://doi.org/10.1021/acs.jpcc.5c05004
J. Phys. Chem. C XXXX, XXX, XXX−XXX

suggesting that more complex redox processes take place during radiolysis.

We can consider the metal reduction as a competition among different radicals. The kinetics is not the same as in the solution, since atoms have a limited capacity to move. However, the trends for interactions between different species should be similar. For example, it was shown that in solution, Cr(III) does not interact with •OH radicals, but its hydrolyzed form, $Cr(OH)^{2+}$, does. In this case, Cr(III) oxidizes to Cr(VI).[51,52] Similarly, $Fe(OH)^{2+}$ reacts much faster with the hydrogen radical in solution than Fe(III).[53,54] Continuing this logic, our hydroxides should be really good in capturing these radicals because they are very hydrolyzed forms of Cr(III) and Fe(III). The difference between the mechanisms that involve Fe(III) and Cr(III) ion scavenging ability is that all Fe(III) will interact with free electrons, reducing to Fe(II), while Cr(III) ions can also interact with oxygen-centered radicals to cause a decrease in the intensity of the signal from oxygen-centered radicals. Oxidized chromium, though, can further react with free electrons, causing further scavenging, which would make it much harder to detect a significant presence of oxidized or reduced Cr ions.

CONCLUSIONS

Transition-metal ions doped into the crystal structure of minerals can act as electron scavengers, changing the quantity and speciation of radiolytic products. Thus, the presence of these trace metals associated with aluminum-bearing phases in radioactive tank waste needs to be accounted for during storage, retrieval, and processing. The incorporation of Cr(III) or Fe(III) ions into gibbsite led to a decrease in H_2 production and the corresponding reduction of the transition metal. The latter is due to the scavenging of electrons from radiolysis, indicating that there is a role for these electrons in the production of H_2 during the radiolysis of gibbsite. The results also show that impurities in gibbsite can have a significant influence on the outcome of radiolysis in radioactive tank waste.

ASSOCIATED CONTENT

Supporting Information

The Supporting Information is available free of charge at https://pubs.acs.org/doi/10.1021/acs.jpcc.5c05004.

High-resolution XPS spectra, pXRD patterns, diffuse-reflectance spectra, EPR spectra, and integrated decay curves of NO_3-gibbsite samples. Ordering information is given on any masthead page (PDF)

AUTHOR INFORMATION

Corresponding Author

Jay A. LaVerne − *Radiation Laboratory, University of Notre Dame, Notre Dame, Indiana 46556, United States; The Department of Physics and Astronomy, University of Notre Dame, Notre Dame, Indiana 46556, United States;* orcid.org/0000-0002-8383-7476; Email: laverne.1@nd.edu

Authors

Hanna Hlushko − *Radiation Laboratory, University of Notre Dame, Notre Dame, Indiana 46556, United States; Idaho National Laboratory, Idaho Falls, Idaho 83405, United States*

Alejandro Ramos-Ballesteros − *Radiation Laboratory, University of Notre Dame, Notre Dame, Indiana 46556, United States; Idaho National Laboratory, Idaho Falls, Idaho 83405, United States*

Amita Bedar − *Radiation Laboratory, University of Notre Dame, Notre Dame, Indiana 46556, United States*

Ping Chen − *Pacific Northwest National Laboratory, Richland, Washington 99354, United States*

Xin Zhang − *Pacific Northwest National Laboratory, Richland, Washington 99354, United States;* orcid.org/0000-0003-2000-858X

Roberto Colina Ruiz − *Pacific Northwest National Laboratory, Richland, Washington 99354, United States*

Kevin M. Rosso − *Pacific Northwest National Laboratory, Richland, Washington 99354, United States;* orcid.org/0000-0002-8474-7720

Carolyn Pearce − *Pacific Northwest National Laboratory, Richland, Washington 99354, United States;* orcid.org/0000-0003-3098-1615

Complete contact information is available at: https://pubs.acs.org/10.1021/acs.jpcc.5c05004

Notes

The authors declare no competing financial interest.

ACKNOWLEDGMENTS

This research was supported as a part of Ion Dynamics in Radioactive Environments and Materials (IDREAM), an Energy Frontier Research Center funded by the U.S. Department of Energy, Office of Science, Basic Energy Sciences (FWP 68932). The authors thank Dr. Hans-Gert Korth of the Universität Duisburg-Essen for identification of the EPR signal of the nitrogen oxide species as the NO_2 radical. The authors thank Prof. Ian Carmichael for making available the facilities of the Notre Dame Radiation Laboratory, which is supported by the Division of Chemical Sciences, Geosciences and Biosciences, Basic Energy Sciences, Office of Science, United States Department of Energy through grant number DE-FC02-04ER15533. This contribution is NDRL-5475 from the Notre Dame Radiation Laboratory. The draft of this paper was prepared with the support of the postdoctoral development program provided through Idaho National Laboratory by the DOE Idaho Operations Office, Contract DE-AC07-05ID14517 with Battelle Energy Alliance, LLC. A portion of the work was carried out in the Environmental and Molecular Sciences Laboratory (EMSL), a national scientific user facility at PNNL sponsored by the DOE Office of Biological and Environmental Research, under user proposals 61223 (10.46936/lsr.proj.2024.61223/60012698) and 51382 (10.46936/lser.proj.2020.51382/60000186). PNNL is a multi-program national laboratory operated by Battelle Memorial Institute under contract no. DE-AC05-76RL01830 for the DOE.

REFERENCES

(1) Eidelpes, E.; Jarrell, J. J.; Lister, T. E.; Horne, G. P.; Parker-Quaife, E. H.; Conrad, J. K.; Pilgrim, C. D.; Abboud, A. W.; Winston, P. L.; Smith, R. E.; et al. Technical basis for extended dry storage of aluminum-clad spent nuclear fuel. *J. Nucl. Mater.* **2023**, *577*, No. 154299.

(2) Page, J. S.; Reynolds, J. G.; Cooke, G. A.; Wells, B. E. Large cemented gibbsite agglomerates in alkaline nuclear waste at the

Hanford site and the impacts to remediation. *J. Hazard. Mater.* **2020**, *384*, No. 121318.
(3) Herting, D. L.; Reynolds, J. G.; Barton, W. B. Conversion of Coarse Gibbsite Remaining in Hanford Nuclear Waste Tank Heels to Solid Sodium Aluminate $NaAl(OH)_4$ x $1.5H_2O$. *Ind. Eng. Chem. Res.* **2014**, *53* (36), 13833−13842.
(4) LaVerne, J. A.; Tandon, L. H_2 Production in the Radiolysis of Water on CeO_2 and ZrO_2. *J. Phys. Chem. B* **2002**, *106* (2), 380−386.
(5) LaVerne, J. A.; Tandon, L. H_2 Production in the Radiolysis of Water on UO_2 and Other Oxides. *J. Phys. Chem. B* **2003**, *107*, 13623−13628.
(6) Skotnicki, K.; Bobrowski, K. Molecular hydrogen formation during water radiolysis in the presence of zirconium dioxide. *J. Radioanal. Nucl. Chem.* **2015**, *304* (2), 473−480.
(7) LaVerne, J. A.; Huestis, P. L. H Atom Production and Reaction in the Gamma Radiolysis of Thermally Modified Boehmite. *J. Phys. Chem. C* **2019**, *123* (34), 21005−21010.
(8) LaVerne, J. A. H_2 Formation from the Radiolysis of Liquid Water with Zirconia. *J. Phys. Chem. B* **2005**, *109* (12), 5395−5397.
(9) Hlushko, H.; Huestis, P. L.; LaVerne, J. A. Silicon and Zirconium Ceramics Radiolysis in the Presence of Water. *J. Phys. Chem. C* **2023**, *127*, 3194−3203.
(10) Wang, Z. M.; Walter, E. D.; Sassi, M.; Zhang, X.; Zhang, H. L.; Li, X. H. S.; Chen, Y.; Cui, W. W.; Tuladhar, A.; Chase, Z.; et al. The Role of Surface Hydroxyls on the Radiolysis of Gibbsite and Boehmite Nanoplatelets. *J. Hazard. Mater.* **2020**, *398*, No. 122853.
(11) Petrik, N. G.; Alexandrov, A. B.; Vall, A. I. Interfacial Energy Transfer During Gamma Radiolysis of Water on the Surface of ZrO_2 and Some other Oxides. *J. Phys. Chem. B* **2001**, *105*, 5935−5944.
(12) Deskins, N. A.; Kimmel, G. A.; Petrik, N. G. Observation of Molecular Hydrogen Produced from Bridging Hydroxyls on Anatase TiO_2(101). *J. Phys. Chem. Lett.* **2020**, *11* (21), 9289−9297.
(13) Lund, A.; Shiotani, M.; Shimada, S. *Principles and Applications of ESR Spectroscopy*; Springer Science & Business Media, 2011.
(14) Hlushko, H.; Ramos-Ballesteros, A.; Chen, P.; Zhang, X.; Rosso, K. M.; Pearce, C. I.; LaVerne, J. A. Effect of impurities on radical formation in gibbsite radiolysis. *Phys. Chem. Chem. Phys.* **2024**, *26* (13), 9867−9870.
(15) Kaddissy, J. A.; Esnouf, S.; Saffre, D.; Renault, J. P. Efficient Hydrogen Production from Irradiated Aluminum Hydroxides. *Int. J. Hydrog. Energy* **2019**, *44* (7), 3737−3743.
(16) Vedrine, J. C.; Imelik, B.; Derouane, E. G. Influence of Physical State of 3 Different Aluminum Hydroxides on Interaction Between Trapped H Atom and Lattice Protons - EPR and ENDOR Studies. *J. Magne. Reson.* **1974**, *16* (1), 95−109.
(17) Kaddissy, J. A.; Esnouf, S.; Durand, D.; Saffre, D.; Foy, E.; Renault, J. P. Radiolytic Events in Nanostructured Aluminum Hydroxides. *J. Phys. Chem. C* **2017**, *121* (11), 6365−6373.
(18) Briley, E.; Huestis, P.; Zhang, X.; Rosso, K. M.; LaVerne, J. A. Radiolysis of thermally dehydrated gibbsite. *Mater. Chem. Phys.* **2021**, *271*, No. 124885.
(19) Kuruc, J. Paramagnetic Centers by X-ray-Irradaition of Aluminum Hydroxide - EPR Spectroscopy, Radiation Chemical-Yield and Kinetics of Thermal Decay of Paramagnetic Centers. *J. Radioanal. Nucl. Chem.-Lett.* **1991**, *154* (1), 61−72.
(20) Huestis, P. L.; Graham, T. R.; Mergelsberg, S. T.; LaVerne, J. A. Identification of Radiolytically-Active Thermal Transition Phases in Boehmite. *Therm. Acta* **2020**, *689*, No. 178611.
(21) Kir'yanov, A. V. Effects of Electron Irradiation Upon Absorptive and Fluorescent Properties of Some Doped Optical Fibers. In *Radiation Effects in Materials*; Monteiro, W. A., Ed.; IntechOpen, 2016.
(22) Reed, D. T.; Bonar, S. D.; Weiner, M. F. Gamma and Alpha Radiation Levels in a Basalt High-Level Waste Repository: Potential Impact on Container Corrosion and Packing Properties. In *Coupled Processes Associated with Nuclear Waste Repositories*; Tsang, C. F., Ed.; Academic Press, 1987; pp 325−335.
(23) Westesen, A.; Peterson, R. Speciation of aluminum phases at the Hanford Site. *Environ. Prog. Sustainable Energy* **2022**, *41* (1), No. e13789.
(24) Zhao, Y.; Prange, M. P.; Zong, M.; Wang, Y.; Walter, E. D.; Chen, Y.; Zhu, Z.; Engelhard, M. H.; Wang, X.; Zhao, X.; et al. Understanding Trace Iron and Chromium Incorporation During Gibbsite Crystallization and Effects on Mineral Dissolution. *Environ. Sci. Technol.* **2024**, *58* (45), 20125−20136.
(25) Zhang, H.; Wang, Z.; Zhao, Y. B.; Cui, W.; Zhang, X.; Wang, S.; Walter, E. D.; Sassi, M. J.; Pearce, C. I.; Clark, S. B.; Rosso, K. M. Metal Ion (Cr^{3+}, Eu^{3+}. UO_2^{2+}) Adsorption on Gibbsite Nanoplates. *Eng. Sci.* **2023**, *24*, No. 896.
(26) Chatterjee, S.; Conroy, M. A.; Smith, F. N.; Jung, H. J.; Wang, Z.; Peterson, R. A.; Huq, A.; Burtt, D. G.; Ilton, E. S.; Buck, E. C. Can Cr(III) substitute for Al(III) in the structure of boehmite? *RSC Adv.* **2016**, *6* (109), 107628−107637.
(27) Cui, W.; Zhang, X.; Pearce, C. I.; Chen, Y.; Zhang, S.; Liu, W.; Engelhard, M. H.; Kovarik, L.; Zong, M.; Zhang, H.; et al. Cr(III) Adsorption by Cluster Formation on Boehmite Nanoplates in Highly Alkaline Solution. *Environ. Sci. Technol.* **2019**, *53* (18), 11043−11055.
(28) Cui, W.; Zhang, X.; Pearce, C. I.; Engelhard, M. H.; Zhang, H.; Wang, Y.; Heald, S. M.; Zheng, S.; Zhang, Y.; Clark, S. B.; et al. Effect of Cr(III) Adsorption on the Dissolution of Boehmite Nanoparticles in Caustic Solution. *Environ. Sci. Technol.* **2020**, *54* (10), 6375−6384.
(29) Zhang, X.; Huestis, P. L.; Pearce, C. I.; Hu, J. Z.; Page, K.; Anovitz, L. M.; Aleksandrov, A. B.; Prange, M. P.; Kerisit, S.; Bowden, M. E.; et al. Boehmite and Gibbsite Nanoplates for the Synthesis of Advanced Alumina Products. *ACS Appl. Nano Mater.* **2018**, *1* (12), 7115−7128.
(30) Gota, S.; Gautier-Soyer, M.; Sacchi, M. Fe 2p absorption in magnetic oxides:: Quantifying angular-dependent saturation effects. *Phys. Rev. B* **2000**, *62* (7), No. 4187.
(31) Zhao, X. D.; Guillen, T. R.; Guillen, T. R.; Graham, T. R.; Chen, P.; Zhao, Y. T.; Mergelsberg, S. T.; Zhu, Z. H.; Wang, Z. M.; Rosso, K. M.; Guo, X. F. Incorporation of rare earth elements Sc, Y and La into gibbsite. *Chem. Eng. J.* **2024**, *485*, No. 149809.
(32) Lin, Y. C.; Chen, Y. Y.; Yu, B. Y.; Lin, W. C.; Kuo, C. H.; Shyue, J. J. Sputter-induced chemical transformation in oxoanions by combination of C_{60}^+ and Ar^+ ion beams analyzed with X-ray photoelectron spectrometry. *Analyst* **2009**, *134* (5), 945−951.
(33) McIntyre, J. F.; Foley, R. T.; Brown, B. F. Ultraviolet-Spectra of Aluminum Salt-Solutions. *Inorg. Chem.* **1982**, *21* (3), 1167−1172.
(34) Liu, S.-T.; Su, T.; Zhang, P.; Fei, Z.-J.; Liu, H.-T. Identification of Superoxide O_2^- During Thermal Decomposition of Molten KNO_3-$NaNO_2$-$NaNO_3$ Salt by Electron Paramagnetic Resonance and UV-Vis Adsorption Spectroscopy. *Chin. J. Chem. Phys.* **2017**, *30*, 372−378.
(35) Ramos-Ballesteros, A.; Gakhar, R.; Horne, G. P.; Iwamatsu, K.; Wishart, J. F.; Pimblott, S. M.; LaVerne, J. A. Gamma radiation-induced defects in KCl, $MgCl_2$, and $ZnCl_2$ salts at room temperature. *Phys. Chem. Chem. Phys.* **2021**, *23* (17), 10384−10394.
(36) Khan, A. U.; Mahanti, S. D. Collective electron effects of O_2^- in potassium superoxide. *J. Chem. Phys.* **1975**, *63* (6), 2271−2278.
(37) Sant'Anna, R. T. P.; Santos, C. M.; Silva, G. P.; Ferreira, R. J.; Oliveira, A. P.; Côrtes, C. E.; Faria, R. B. Kinetics and mechanism of chlorate-chloride reaction. *J. Braz. Chem. Soc.* **2012**, *23*, 1543−1550.
(38) Samdani, M.; Ramadevudu, G.; Chary, M. N.; Shareefuddin, M. EPR, Optical and Physical Studies on Cr^{3+} Doped MgO−BaO−B_2O_3−TeO_2 Glasses. *St. Petersburg Polytech. Univ. J.: Phys. Math.* **2017**, *3* (4), 299−307.
(39) Gispert, J. R. *Coordination chemistry*; Wiley-VCH Weinheim, 2008.
(40) Stuenzi, H.; Marty, W. Early Stages of the Hydrolysis of Chromium(III) in Aqueous Solution. 1. Characterization of a Tetrameric Species. *Inorg. Chem.* **1983**, *22* (15), 2145−2150.
(41) Elliot, A. J.; Sopchyshyn, F. C. The Radiolysis at Room Temperature and 118C of Aqueous Solutions Containing Sodium Nitrate and Either Sodium Formate or 2-Propanol. *Can. J. Chem.* **1983**, *61*, 1578−1582.

https://doi.org/10.1021/acs.jpcc.5c05004
J. Phys. Chem. C XXXX, XXX, XXX−XXX

(42) Giamello, E.; Rumori, P.; Geobaldo, F.; Fubini, B.; Paganini, M. C. The interaction between hydrogen peroxide and metal oxides: EPR investigations. *Appl. Magne. Reson.* **1996**, *10* (1−3), 173−192.
(43) Amorelli, A.; Evans, J. C.; Rowlands, C. C. An Electron-Spin Resonance Study of the Superoxide Radical-Anion in Polycrystalline Magnesium-Oxide and Titanium-Dioxide Powders. *JJ. Chem. Soc., Faraday Trans. I* **1988**, *84*, 1723−1728.
(44) Drago, R. S. *Physical Methods for Chemists*; Saunders College Pub., 1992.
(45) Bonomo, R. P.; Di Bilio, A. J.; Riggi, F. EPR Investigation of Chromium (III) Complexes: Analysis of Their Frozen Solution and Magnetically Dilute Powder Spectra. *Chem. Phys.* **1991**, *151* (3), 323−333.
(46) Theil, C.; van Elp, J.; Folkmann, F. Ligand field parameters obtained from and chemical shifts observed at the Cr $L_{2,3}$ edges. *Phys. Rev. B* **1999**, *59* (12), No. 7931.
(47) Giménez-Marqués, M.; Bellido, E.; Berthelot, T.; Simón-Yarza, T.; Hidalgo, T.; Simón-Vázquez, R.; González-Fernández, A.; Avila, J.; Asensio, M. C.; Gref, R.; et al. GraftFast Surface Engineering to Improve MOF Nanoparticles Furtiveness. *Small* **2018**, *14* (40), No. 1801900.
(48) Huestis, P.; Pearce, C. I.; Zhang, X.; N'Diaye, A. T.; Rosso, K. M.; LaVerne, J. A. Radiolytic stability of gibbsite and boehmite with adsorbed water. *J. Nucl. Mater.* **2018**, *501*, 224−233.
(49) Westbrook, M. L.; Sindelar, R. L.; Fisher, D. L. Radiolytic Hydrogen Generation from Aluminum Oxyhydroxide Solids: Theory and Experiment. *J. Radioanal. Nucl. Chem.* **2015**, *303*, 81−86.
(50) Atkins, P. W. *Physical Chemistry*, 4th ed.; W. H. Freeman and Company, 1990.
(51) Conrad, J. K.; Lisouskaya, A.; Mezyk, S. P.; Bartels, D. M. Kinetics of the Temperature-Dependent e_{aq}^- and •OH Radical Reactions with Cr(III) Ions in Aqueous Solutions. *ChemPhysChem* **2023**, *24* (24), No. e202300465.
(52) Djouider, F.; Hussain, A. A laboratory study of the oxidation of non toxic Cr(III) to toxic Cr(VI) by OH• free radicals in simulated atmospheric water droplets conditions: Potential environmental impact. *J. Hazard. Mater.* **2015**, *283*, 905.
(53) Baxendale, J. H.; Dixon, R. S.; Stott, D. A. Reactivity of hydrogen atoms with Fe^{3+} $FeOH^{2+}$ and Cu^{2+} in aqueous solutions. *Trans. Faraday Soc.* **1968**, *64*, 2398−2401.
(54) Navon, G.; Stein, G. Reactivity of some high- and low-spin iron(3) complexes with atomic hydrogen in aqueous solution. *J. Phys. Chem. A* **1966**, *70* (11), 3630−3641.

https://doi.org/10.1021/acs.jpcc.5c05004
J. Phys. Chem. C XXXX, XXX, XXX−XXX